buildings

MDPI

Article

An Experimental Study on the Effect of Nanomaterials and Fibers on the Mechanical Properties of Polymer Composites

Chanachai Thongchom [1], Nima Refahati [2,*], Pouyan Roodgar Saffari [1,*], Peyman Roudgar Saffari [3], Meysam Nouri Niyaraki [4], Sayan Sirimontree [1] and Suraparb Keawsawasvong [1]

[1] Department of Civil Engineering, Faculty of Engineering, Thammasat School of Engineering, Thammasat University, Pathumthani 12120, Thailand; Tchanach@engr.tu.ac.th (C.T.); ssayan@engr.tu.ac.th (S.S.); ksurapar@engr.tu.ac.th (S.K.)
[2] Department of Mechanical Engineering, Damavand Branch, Islamic Azad University, Damavand P.O. Box 3971878911, Iran
[3] Department of Mechanical Engineering, Adiban Institute of Higher Education, Garmsar P.O. Box 3588143112, Iran; saffari.p86@gmail.com
[4] Faculty of Mechanical Engineering, Semnan University, Semnan P.O. Box 3513119111, Iran; meysam_nouri05@yahoo.com
* Correspondence: refahati@damavandiau.ac.ir (N.R.); poyan.safari31@gmail.com (P.R.S.)

Abstract: This study aims to explore the tensile and impact properties (tensile strength, modulus of elasticity, and impact strength) of polypropylene (PP)-based nanocomposites reinforced with graphene nanosheets, nanoclay, and basalt fibers. The response surface methodology (RSM) with Box–Behnken design (BBD) was adopted as the experimental design. An internal mixer was used to prepare compounds consisting of 0, 0.75 and 1.5 wt% graphene nanosheets, 0, 10 and 20 wt% basalt fibers, and 0, 3 and 6 wt% nanoclay. The samples were prepared by a hot press machine for mechanical testing. The tensile tests were run to determine the tensile strength, and modulus of elasticity, and the Charpy impact tests were performed to assess the impact strength. It was found that the addition of basalt increased the tensile strength, modulus of elasticity, and impact strength by 32%, 64% and 18%, respectively. Also, the incorporation of the low-weight graphene nanosheets increased the tensile and impact strength by 15% and 20%, respectively, Adding graphene nanosheets generally improved the modulus of elasticity by 66%. Similarly, the addition of nanoclay improved the tensile strength by 17% and increased the modulus of elasticity by 59%, but further addition of it decreased the impact strength by 19%. The values obtained by this experiment for the mechanical property were roughly close to the data yielded from desirability optimization.

Keywords: mechanical properties; graphene; nanoclay; basalt; polypropylene; FE-SEM

Citation: Thongchom, C.; Refahati, N.; Roodgar Saffari, P.; Roudgar Saffari, P.; Niyaraki, M.N.; Sirimontree, S.; Keawsawasvong, S. An Experimental Study on the Effect of Nanomaterials and Fibers on the Mechanical Properties of Polymer Composites. *Buildings* **2022**, *12*, 7. https://doi.org/10.3390/buildings12010007

Academic Editors: Daniele Zulli and Valeria Settimi

Received: 5 November 2021
Accepted: 20 December 2021
Published: 23 December 2021

1. Introduction

In recent years, polymer composites have been widely used in industry due to their lightness, resistance, and excellent mechanical properties [1]. These properties have made them more usable than metals [2]. Polypropylene (PP) is an important and widely used thermoplastic due to its light weight, less expensive cost of manufacturing, good heat deflection temperature, and renewability [3,4]. When PP is used at room temperature, it exhibits very good mechanical, thermal, and physical properties. Blending of polymers is often a convenient method for obtaining improved polymeric materials, which are difficult to obtain by direct polymerization processes [5,6]. Nanomaterials are very important in various industries today. Nanomaterials are used in nanocomposites to reinforce them. Examples of these nanomaterials are nanographene, carbon nanotubes, clay nanotubes, and nanosilica [7–9]. Saffari et al. studied the mechanical properties of carbon nanotubes [10–12].

Graphene are a single layer of carbon atoms that are tightly bound, giving a honeycomb-like appearance to graphene sheets. The unique properties of graphene, including high

specific surface area, high young's modulus, a strong filler-matrix interface, and better bonding of the polymer matrix and the filler particles have increased the use of this material [13]. Shokrieh et al. [14] studied the processing and structural characteristics of graphene/PP nanocomposites. It appeared that adding 0.5 wt% graphene to PP improves the modulus of elasticity of PP. Zhang et al. [15] fabricated high-strength graphene-reinforced nanocomposites in net shape for complex 3D structures by digital light processing. They found that by adding 5 wt% of graphene to PP, the modulus of elasticity significantly improved. Hakan et al. [16] assessed the mechanical and thermal properties of PP composites subjected to graphene oxide loading. They concluded that the addition of graphene oxide to PP resulted in a dramatic improvement in tensile strength and Young's modulus by 42% and 71%, respectively. The use of graphene to upgrade the mechanical behaviour of composites was investigated by Wang et al. [17], as well. They tested the samples for tensile, morphological, and thermal properties and found that adding a low content of graphene to the PP improved the tensile properties. Ansari et al. [18] fabricated and compared the mechanical behaviour of PP nanocomposites reinforced with carbon fiber and calcium carbonate nanoparticles. They found that the incorporation of calcium carbonate nanoparticles enhanced the impact strength of nanocomposites compared to those without nanoparticles. They attributed this increase to the structure uniformity and the good adhesion between the two-phase PP and calcium carbonate. Corroborating the findings of this study, Yuan et al. [19] reported that the inclusion of 1 wt% of graphene oxide to PP yielded better tensile properties. Gharebeiglou et al. [20] also examined the mechanical and thermal behavior of PP nanocomposites reinforced with graphene oxide. They concluded that the Young's polymer modulus was improved by adding 0.1%, 0.3%, and 0.5% AGO by 20%, 30%, and 34%, respectively. They also reported that the 10% mass reduction temperature for 0.1%, 0.3%, and 0.5% AGO nanocomposites increased by 2, 8 and 12 °C for pure polypropylene, respectively.

One of the most common nanofillers in polymers is layered silicates. Because of the lower mineral phase, silicate nanocomposites are less heavy than conventional composites and therefore can be used as substitutes for these composites in various applications [21,22]. Liaghat et al. [23] studied the effect of nanoclay incorporation on the energy absorption capacity of steel-polyurea bi-layer plates. They concluded that the inclusion of 1 wt% nanoclay to polyuria led to an increase in the modulus of elasticity by about 60%. Esmizadeh et al. [24] investigated the mechanical behavior of hybrid polyethylene-based nanocomposites reinforced with nanoperlite and nanoclay. They argued that a 7 wt% increase in nanoparticles resulted in a uniform distribution of nanoparticles in the polyethylene matrix and an improved tensile strength, and the modulus of elasticity of the composites with 5 wt% of nanoclay and 2 wt% of nanoperlite was about twice that of pure polyethylene.

Today, fibers are used in many composite materials to reinforcement them against a variety of loads and these fiber reinforced composites are used in many applications in many industries [25–28]. One of the environmentally safe fibers is basalt. Basalt fibers have high flexibility and resilience, high heat tolerance, and adequate corrosion resistance. They have various applications [29]. For instance, in post-earthquake remediation and reinforcement, basalt-reinforced composites are used as external bonding sheets [30,31]. The mechanical properties of basalt-reinforced plastic were studied by Lopresto et al. [32]. They used vacuum technology to prepare their samples and a universal machine to do tensile testing. They found that reinforcement with basalt yielded better mechanical properties than reinforcement with alternative fibers. Wang et al. [33] examined the resistance and the fatigue behavior of composites reinforced with carbon fiber, glass fiber, and basalt fiber. They concluded that carbon/basalt composites increased the potential for fatigue tolerance. The characterization of modern basalt-reinforced composites was studied by Colombo et al. [34]. They argued that composites reinforced with epoxy resin had stronger mechanical properties than those reinforced with vinyl ester. High et al. [35] used basalt for the reinforcement of concrete. It appeared that the flexural structure of basalt-reinforced concrete provided high compressive strength of the concrete and acceptable serviceability.

Shishevan et al. [36] examined the behavior of basalt-reinforced polymer composites. They focused on the main parameters of low-velocity impact, including energy absorption, initial maximum force, and deformation, and compared them with polymer plates reinforced with carbon fibers. Their results showed that, owing to the high toughness of basalt fibers, the plates reinforced with these fibers showed much better performance compared to those reinforced with carbon fibers.

Another significant benefit of basalt fibers is their manufacturing, which uses fewer resources and is less expensive than glass or carbon fibers [37,38]. Eslami et al. [39] investigated the mechanical behavior of PP/clay nanocomposites reinforced with basalt. They argued that, owing to the high resilience of basalt, the final strength and modulus of elasticity increased dramatically. The mechanical properties of basalt-reinforced polymers were examined by Chen et al. [40]. The findings revealed that the samples yielded tensile stress, fracture strain, and modulus of elasticity of 1642.2 MPa, 0.021, and 77.9 GPa, respectively.

In this research, the mechanical behavior of PP nanocomposites reinforced with graphene, nanoclay, and basalt fibers has been investigated. The aim of this research is to obtain a polymer nanocomposite with maximum levels of tensile strength, modulus of elasticity, and impact strength.

2. Materials and Method

2.1. Materials

This study used PP (v30s trade name) as a matrix. It had a melt index of 18 g/10 min and a density of 0.918 g/cm^3, and was manufactured and purchased from Arak Petrochemical Company (Boshehr, Iran).

In this study XGnP-C750 graphene nanosheets were supplied by XG Science (Lansing, USA) with a minimum thickness of 2 nm, an average diameter of below 2 mm, and an average surface area of 750 m^2/g. A further reinforcement utilized in this study was basalt, which was provided by Basaltex Company (Wevelgem, Belgium), with a density of 300 g/cm^3 with an average diameter of 14 nm, the average length of 6 mm. Also, modified montmorillonite nanoclay with a tensile strength of 101 MPa and impact strength of 27 J/m was used.

2.2. Preparation of Samples

In general, the materials were combined to produce the tensile and impact test specimens. An internal mixer type HBI SYS 90 (Vreden, Germany) with a speed of 60 rpm at 180 °C was used to mix the polymer and reinforcements for 10 min. A hot compression molding machine with a square steel mold (250 m × 250 m) was used to prepare the samples at a temperature of 190 °C. The pre-heating temperature of the platens was 190 °C, and a minimum level of pressure was exerted in this phase to keep the contact between the platens and the mold. Subsequently, the pressure was then gradually elevated to 2.5 MPa for 2 min and kept constant for a further 5 min. Subsequently, keeping the pressure constant, the mold was transferred to a cold press and cooled down to room temperature (2.5 MPa). Compounds included graphene (at 0, 0.75 and 1.5 wt%), basalt fibers (at 0, 10, and 20 wt%), and nanoclay (at 0, 3 and 6 wt%).

2.3. Characterization

The tensile test was run based on ISO 527-1 to determine the tensile strength and modulus of elasticity. The dimension of tensile samples is 3.2 mm in thickness, 19 mm in width, 115 mm in length and 6 mm in width of the narrow section. The tensile test was performed using a Zwick/Roell (Byronas, Greece). The Charpy impact test was run at room temperature based on ISO 179 standard for grooved samples with the groove angle and depth of 45° and 2.5 mm, respectively. The dimension of the impact samples is 3.2 mm in thickness, 12.7 mm in width and 63.5 mm in length. The tensile and impact test machine is shown in Figure 1. A field emission scanning electron microscope (FE-SEM) was applied to scan the samples' fracturing surface. To obtain more accurate results, each combination

was tested five times. At the end, the average of tests was also reported for tensile strength, modulus of elasticity, and impact strength. Figure 2 indicates samples before and after running the tests.

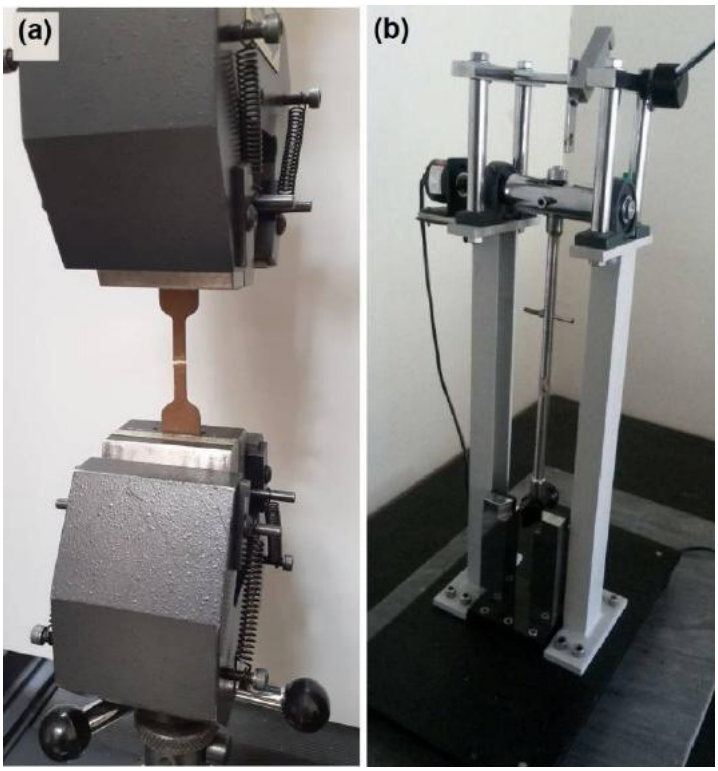

Figure 1. (**a**) Tensile test machine and (**b**) Charpy impact test machine.

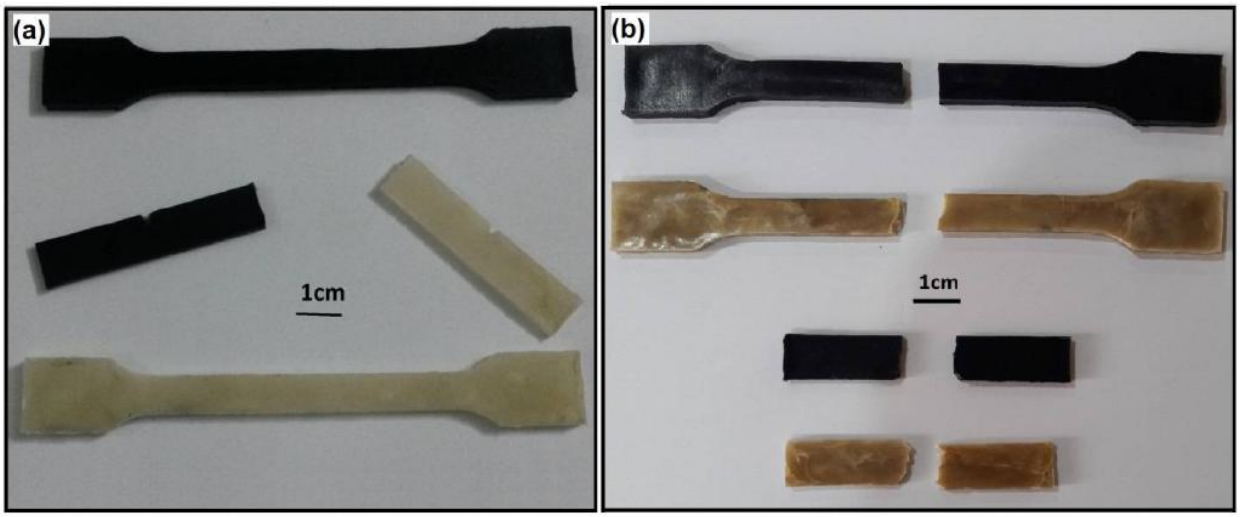

Figure 2. Tensile and Impact test samples: (**a**) before testing and (**b**) after testing.

3. Design of Experiment

The regression model employing response surface methodology (RSM) with Box–Behnken design (BBD) was adopted in this study. According to studies conducted by other researchers, The design included three variables, each at three levels (graphene (at 0, 0.75 and 1.5 wt%), nanoclay (at 0, 3 and 6 wt%), and basalt (at 0, 10 and 20 wt%)), as shown in Table 1.

Table 1. Variables and levels in Box–Behnken experimental design.

Variables (wt%)	Low (−1)	Middle (0)	High (1)	Reference
Graphene (X_1)	0	0.75	1.5	[41,42]
Nanoclay (X_2)	0	3	6	[24,39]
Basalt (X_3)	0	10	20	[31,32]

To model the answer given in Equation (1), a quadratic polynomial is typically used.

$$Y = \alpha_0 + \alpha_1 X_1 + \alpha_2 X_2 + \alpha_3 X_3 + \alpha_{11} X_1^2 + \alpha_{22} X_2^2 + \alpha_{33} X_3^2 + \alpha_{12} X_1 X_2 + \alpha_{13} X_1 X_3 + \alpha_{23} X_2 X_3 \quad (1)$$

where Y is the response; X_1, X_2, and X_3 are the variables; α_0 is the amount term; α_1, α_2 and α_3 are the coefficients of the polynomial linear effects; α_{11}, α_{22} and α_{33} are the coefficients of quadratic effect; and α_{12}, α_{13} and α_{23} are the coefficients of the polynomial interaction effect [43].

4. Results and Discussion

According to the Box–Behnken DOE, 15 experiments including three center points were carried out, as given in Table 2. Table 3 shows the results for modulus of elasticity, tensile, and impact strength for 15 samples prepared following tensile and impact testing. Also, to investigate the effect of each variable on the mechanical properties of pure polypropylene, samples 16 to 22 were made and the results for modulus of elasticity, tensile, and impact strength are shown in Table 4.

Table 2. Experimental design for samples.

Sample Code	1	2	3	4	5	6	7	8	9	10	11	12	13	14	15
Graphene (wt%)	0	1. 5	0	1. 5	0	1. 5	0	1. 5	0.75	0.75	0.75	0.75	0.75	0.75	0.75
Nanoclay (wt%)	0	0	6	6	3	3	3	3	0	6	0	6	3	3	3
Basalt (wt%)	10	10	10	10	0	0	20	20	0	0	20	20	10	10	10
PP (wt%)	90	88.5	84	82.5	97	95.5	77	75.5	99.25	93.25	79.25	73.25	86.25	86.25	86.25

Table 3. Experimental result for modulus of elasticity, tensile, and impact strength.

Experiment Run	1	2	3	4	5	6	7	8	9	10	11	12	13	14	15
Tensile strength (MPa)	24.5	26.8	25.9	28.0	25.4	27.7	29.6	31.7	25.6	26.9	29.6	30.9	30.6	30.5	30.4
Modulus of elasticity (GPa)	1.35	2.65	2.25	3.55	0.95	2.25	2.75	4.05	1.25	2.40	3.20	3.70	2.95	2.90	2.85
Impact strength (J/m)	78	86	72	81	69	81	81	88	84	80	97	89	92	90	91

Table 4. Effect of each variable on the mechanical properties of pure polypropylene.

Experiment Run	16	17	18	19	20	21	22
Graphene (wt%)	0	0.75	1.5	0	0	0	0
Nanoclay (wt%)	0	0	0	3	6	0	0
Basalt (wt%)	0	0	0	0	0	10	20
PP (wt%)	100	99.25	98.5	97	94	90	80
Tensile strength (MPa)	22.6	26	25.2	26.3	24	26.3	30
Modulus of elasticity (GPa)	0.6	0.8	1	0.75	0.95	0.8	1.1
Impact strength (J/m)	72	85	80	68	60	78	84

4.1. Morphology

FE-SEM micrographs of the fracture surface of samples in liquid nitrogen were shown in Figures 3–7. Figure 3 shows the fracture surface micrographs of a sample containing 0.75 wt% graphene, 3 wt% nanoclay, and 10 wt% basalt (sample number 13) after tensile test. As shown, for low percentages of graphene and nanoclay, basalt fibers have desirable adhesion to the polymer matrix, decreasing the likelihood of fiber pull-out from the PP

while tensile loading [44]. It has also been observed that the low percentage of graphene and nanoclay has prevented the growth of corrosion pits and cracks bridging, and deflection in the cracks and has improved the mechanical behaviour of the nanocomposite.

Figure 4 displays the fracture surface micrographs of a sample with 0 wt% graphene, 0 wt% nanoclay, and 10 wt% basalt (sample number 1) after tensile test. As shown, due to the absence of graphene and nanoclay, no bond has been established between the fibers and the matrix, and the fiber-matrix adhesion is very weak, leading to fiber pull-out of the matrix while tensile testing. A similar observation has been reported by Nouri et al. [42] which shows a good agreement.

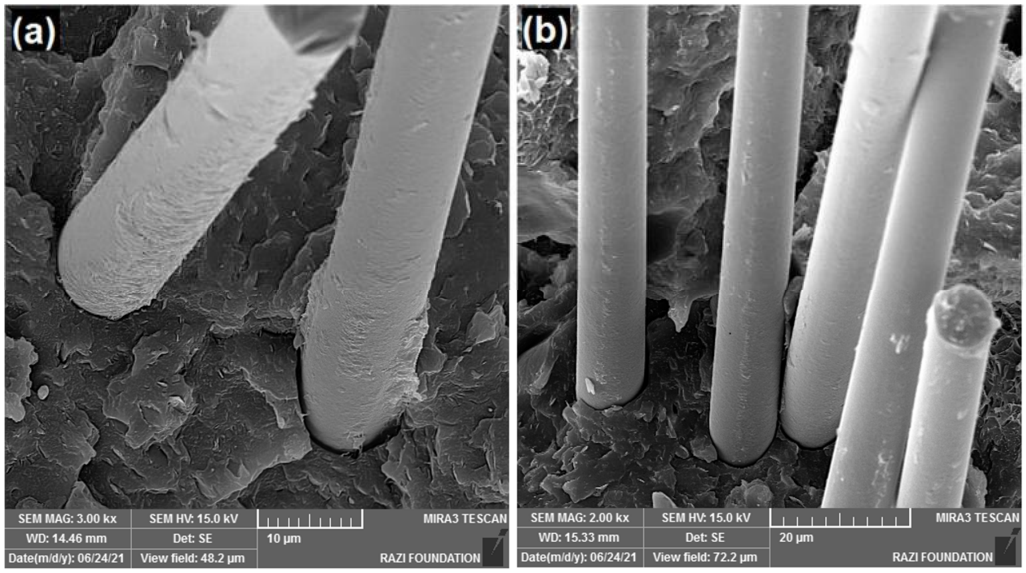

Figure 3. Field-emission scanning electron microscopy (FE-SEM) micrographs of the sample containing 0.75 wt% graphene, 3 wt% nanoclay, and 10 wt% basalt (sample number 13) after tensile test, (**a**) with 3000× magnification, (**b**) with 2000× magnification.

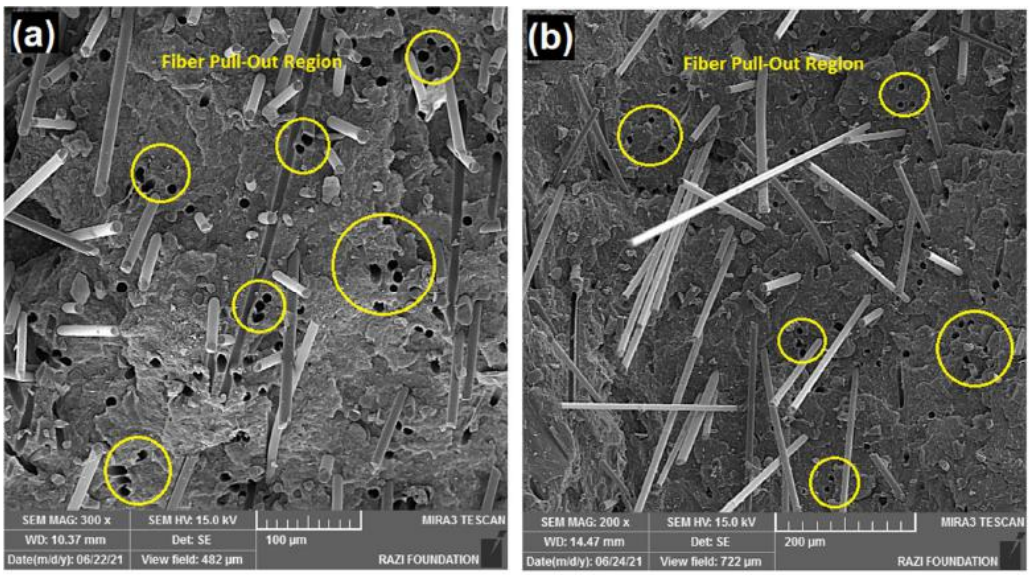

Figure 4. FE-SEM micrographs of the sample containing 0 wt% graphene nanosheets, 0 wt% nanoclay, and 10 wt% basalt (sample number 1) after tensile test, (**a**) under tensile loading, (**b**) under impact loading.

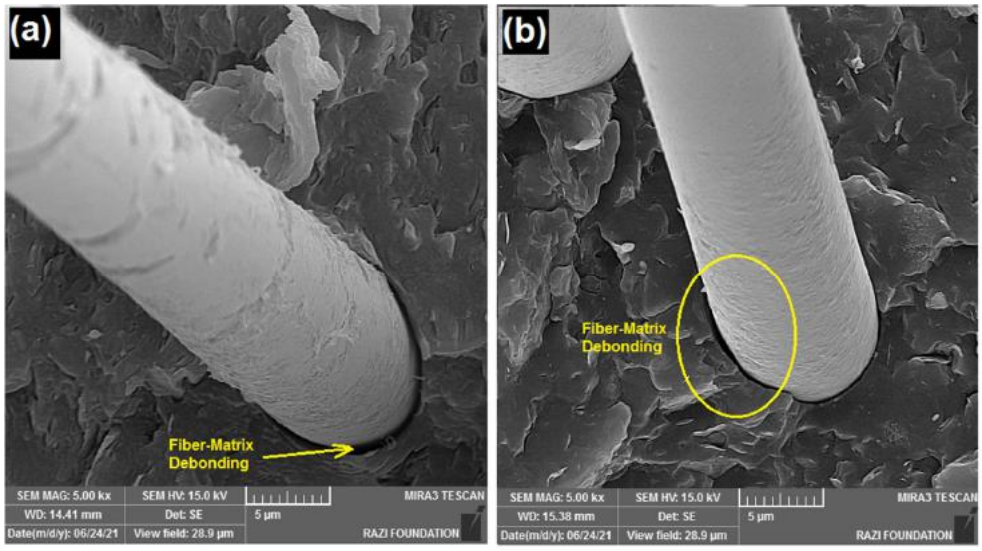

Figure 5. FE-SEM micrographs of the sample containing 0.75 wt% graphene nanosheets, 3 wt% nanoclay, and 10 wt% basalt (sample number 13), (**a**) under tensile loading, (**b**) under impact loading.

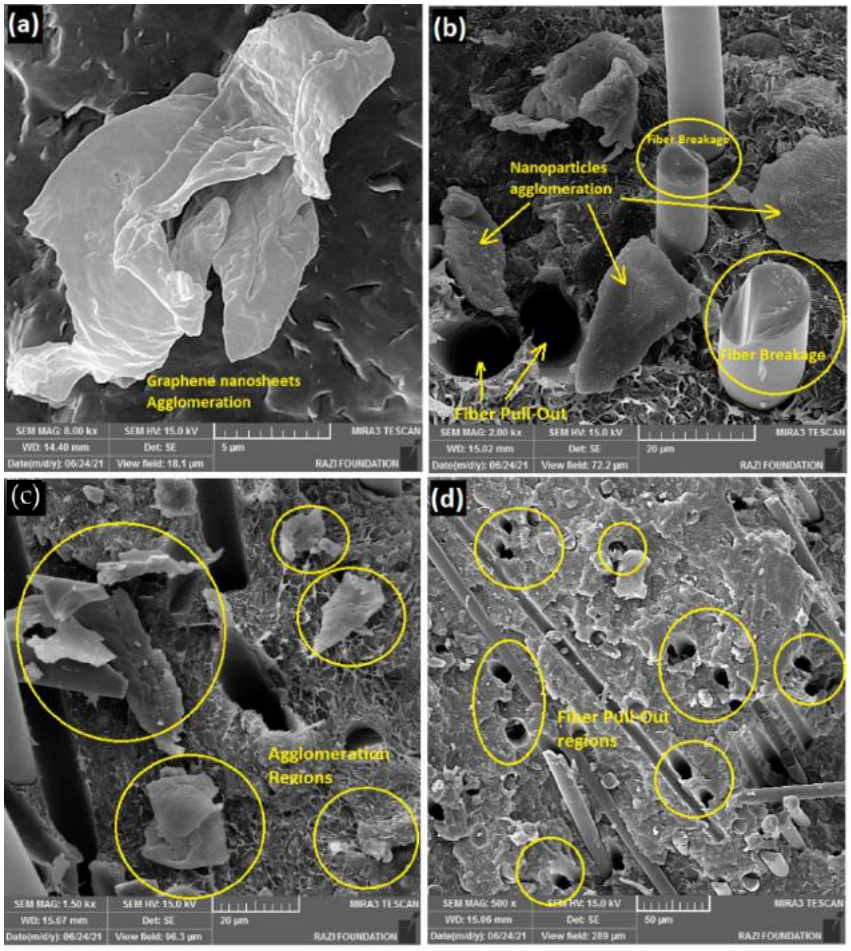

Figure 6. FE-SEM micrographs of the samples containing a high percentage of graphene nanosheets and nanoclay, (**a**) sample number 6 (1.5 wt% graphene nanosheets, 3 wt% nanoclay, and 0 wt% basalt), (**b**) sample number 4 (1.5 wt% graphene nanosheets, 6 wt% nanoclay, and 10 wt% basalt) under tensile loading, (**c**) sample number 4 (1.5 wt% graphene nanosheets, 6 wt% nanoclay, and 10 wt% basalt), and (**d**) sample number 12 (0.75 wt% graphene nanosheets, 6 wt% nanoclay, and 20 wt% basalt).

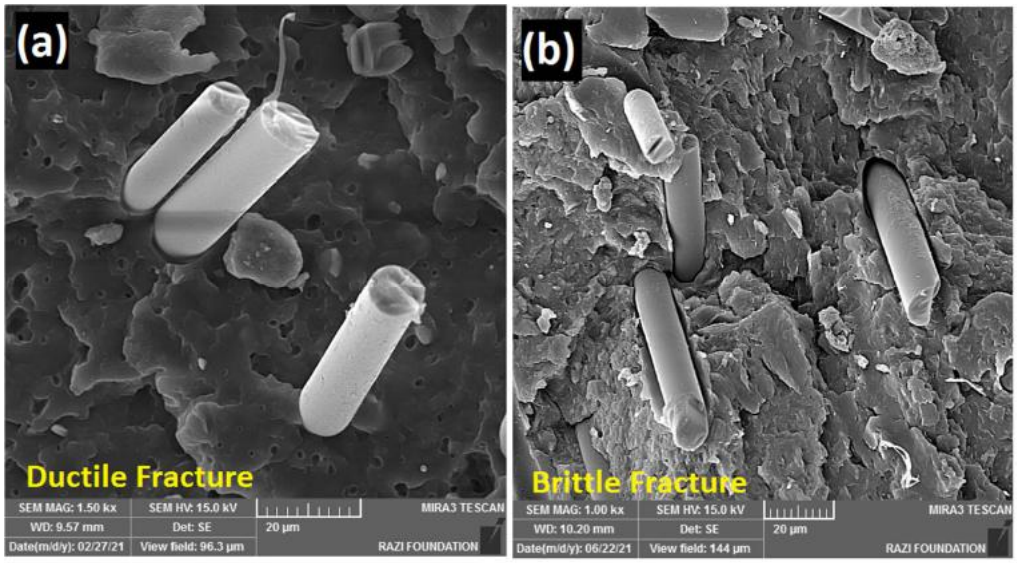

Figure 7. FE-SEM micrographs of ductile and brittle fracture of samples under impact loading. (**a**) Sample number 11 (0.75 wt% graphene nanosheets, 0 wt% nanoclay, and 20 wt% basalt), and (**b**) sample number 3 (0 wt% graphene nanosheets, 6 wt% nanoclay, and 10 wt% basalt).

Figure 5 indicates the fracture surface micrographs of a sample containing 0.75 wt% graphene, 3 wt% nanoclay, and 10 wt% basalt (sample number 13) after impact test. As can be seen, interfacial debonding has occurred between the basalt fibers and the matrix. It is also observed that the fibers are resistant to pulling out and remain in the matrix, leading to load transfer from the matrix to the fibers, and hence fiber breakage. Evidence shows that the high strength of basalt fibers against fracture in comparison to that of pure matrix improves the impact strength of nanocomposites [45,46].

Figure 6 displays the fracture surface micrographs of samples containing a high percentage of graphene and nanoclay. Figure 6a shows the fracture surface micrograph of a sample containing 1.5 wt% graphene, 3 wt% nanoclay, and 0 wt% basalt (sample number 6). As one can see, the graphene are agglomerated and not homogeneously distributed in the polymer matrix. Figure 6b,c show the fracture surface micrographs of a sample containing 1.5 wt% graphene, 6 wt% nanoclay, and 10 wt% basalt (sample number 4) after tensile and impact test, respectively. The figure shows the agglomeration of graphene and nanoclay, which weaken the adhesion between the substrate and the fibers and reduces the tensile properties of the nanocomposites. Figure 6d shows the fracture surface micrograph of a sample containing 0.75 wt% graphene, 6 wt% nanoclay, and 20 wt% basalt (sample number 12) after tensile test. As evident, the agglomeration of graphene and nanoclay diminishes the adhesion between the matrix and the fibers and causes fiber pull-out of the matrix under tensile loading.

Figure 7 indicates the impact of nanoclay addition on the surface fracture under impact loading. Figure 7a shows the fracture surface micrographs of a sample containing 0.75 wt% graphene, 0 wt% nanoclay, and 20 wt% basalt (sample number 11), and Figure 7b shows the fracture surface micrographs of a sample containing 0 wt% graphene, 6 wt% nanoclay, and 10 wt% basalt (sample number 3). As can be seen, the presence of nanoclay resulted in the creation of brittle compounds, which has ultimately reduced the impact strength of the nanocomposites.

4.2. Effect of Graphene, Nanoclay, and Basalt Weight on the Tensile Strength

Figure 8 shows the effect of graphene on tensile strength. As can be seen, the incorporation of graphene up to 0.75 wt% enhanced the tensile strength owing to better adhesion of fibers to the surface in these samples. For higher weights of graphene, however, the tensile strength decreased due to the agglomeration of nanoparticles [44].

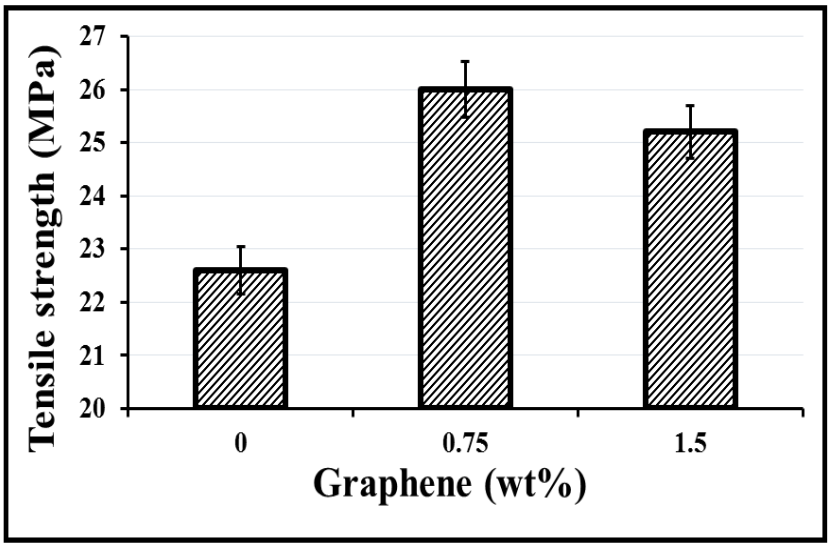

Figure 8. The effect of graphene on the tensile strength.

Figure 9 indicates the effect of nanoclay on the tensile strength. As can be seen, for low weights of nanoclay, the tensile strength increased, but it decreased at a higher weight due to the agglomeration of nanoparticles.

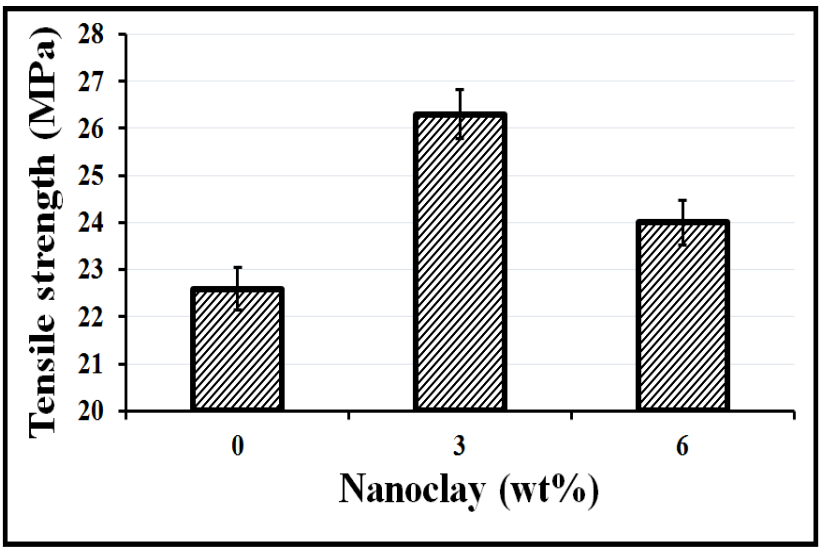

Figure 9. The effect of nanoclay on the tensile strength.

Figure 10 indicates the effect of basalt on tensile strength. As shown, the incorporation of basalt increases the tensile strength, which may be attributed to the fibers' excellent adhesion to the polymer and no pull-out of the matrix during the tensile test [47,48]. Figure 3 (FE-SEM image) shows similar results.

To determine the significant factors affecting the tensile strength of PP/graphene/nanoclay/basalt hybrid nanocomposites, an analysis of variance (ANOVA) was run. The Fisher's value ratio (*F*-value) in the ANOVA test shows that whether the variance between the means of two groups is statistically significant, and the *p*-value shows the probability that the null hypothesis is true [43]. The results of ANOVA for the tensile strength are presented in Table 5. As the table shows, all of the three process parameters' linear (graphene, nanoclay, and basalt) and square [(graphene × graphene) (nanoclay × nanoclay)] coefficients had an effect on tensile strength based on *p*-value. The high values of R^2 (99.97%), R^2_{Adj} (99.91%), and R^2_{Pred} (99.84%) suggest the strong predictability of the model.

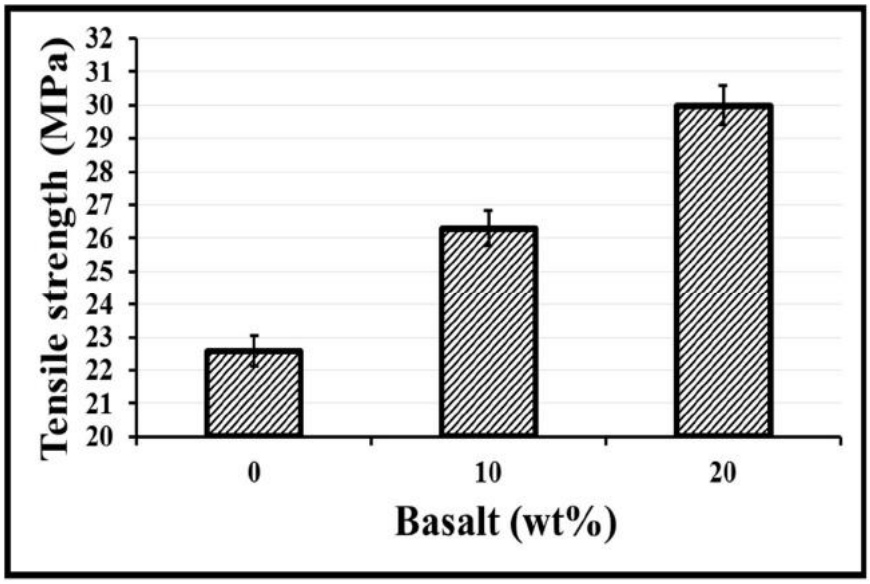

Figure 10. The effect basalt on the tensile strength.

Table 5. Analysis of variance (ANOVA) results for tensile strength.

Source	DF	Adj SS	Adj MS	F	*p*
Model	9	76.76	8.53	1705.87	<0.0001
Graphene (A)	1	9.68	9.68	1936.00	<0.0001
Nanoclay (B)	1	3.38	3.38	676.00	<0.0001
Basalt (C)	1	32.81	32.81	6561.00	<0.0001
Graphene × Nanoclay (AB)	1	0.0100	0.0100	2.00	0.2164
Graphene × Basalt (AC)	1	0.0100	0.0100	2.00	0.2164
Nanoclay × Basalt (BC)	1	0.0000	0.0000	0.0000	1.0000
Graphene × Graphene (A^2)	1	13.68	13.68	2736.46	<0.0001
Nanoclay × Nanoclay (B^2)	1	19.11	19.11	3822.00	<0.0001
Basalt × Basalt (C^2)	1	0.0023	0.0023	0.4615	0.5271
R^2 = 99.97%		R^2_{Adj} = 99.91%		R^2_{Pred} = 99.84%	

The quadratic equation was shown as an Equation (2) in terms of encoded factors after excluding the small variables.

$$S_T = 22.5365 + 6.605A + 1.7346B + 0.20250C - 3.4256A^2 - 0.25299B^2 \quad (2)$$

Figure 11 shows the surface plots and counter plots for tensile strength. Figure 11a indicates the effect of graphene and nanoclay on the tensile strength of the nanocomposite. Figure 11b shows the impact of graphene and basalt, and Figure 11c displays the impact of nanoclay and basalt on the tensile strength of the nanocomposites.

In Figure 11a, for basalt weight of 10 wt%, adding 0.75 wt% of graphene and 3 wt% of nanoclay improved the tensile strength. This is because, at low content of nanoparticles, the adhesion between the fibers and the matrix reaches its highest level, which prevents crack growth and ultimately improves the tensile strength. For higher weight of nanoparticles, the agglomeration of graphene and nanoclay in the compounds decreased the tensile strength [41,42]. Figure 11b illustrates that, by keeping the nanoclay weight at 3 wt%, increasing basalt weight improved the tensile strength, which is attributable to the establishment of good adhesion between the fibers and polymer and no pull-out of the matrix during the tensile test [47,48]. Similarly, the tensile strength increased by adding graphene at 0.75 wt%. This suggests that incorporating a lower content of graphene yields the maximum fiber-matrix adhesion, but higher weights of graphene result in agglomeration and reduce the tensile strength [44].

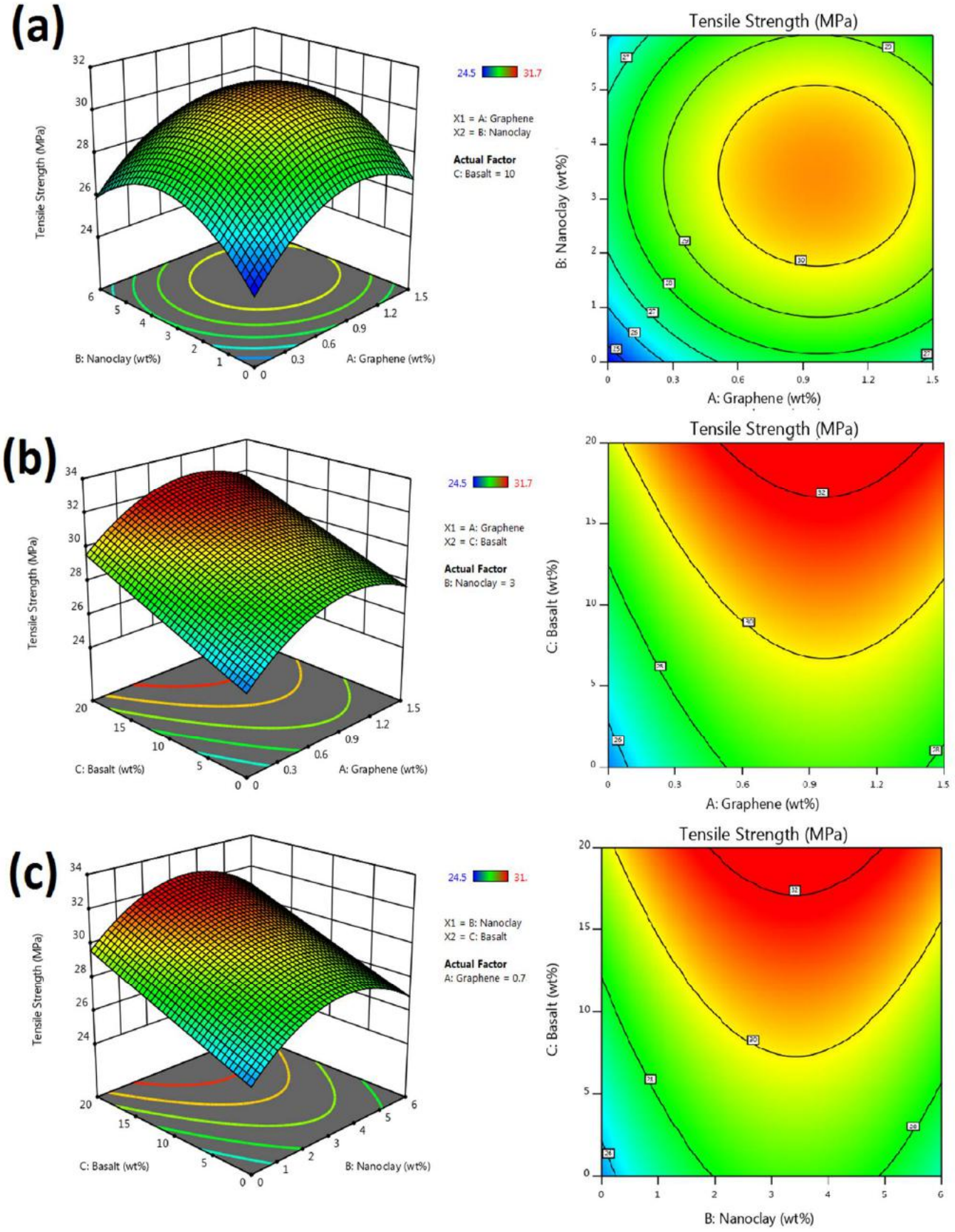

Figure 11. Effect of graphene, nanoclay, and basalt on the tensile strength (**a**) Basalt = 10 wt%, (**b**) Nanoclay = 3 wt%, and (**c**) Graphene = 1 wt%.

In Figure 11c, by keeping the graphene weight at 0.75 wt%, increasing basalt weight increases the tensile strength, and incorporation of nanoclay at 3 wt% leads to an initial increase and then a decrease in tensile strength.

4.3. Effect of Graphene, Nanoclay, and Basalt on the Modulus of Elasticity

Figure 12 indicates the effect of graphene on the modulus of elasticity. As one can see, the addition of graphene nanoparticles to the compounds increases the modulus of elasticity. This may be attributed to a good distribution of graphene and their effective role in building a strong fiber–matrix adhesion [16].

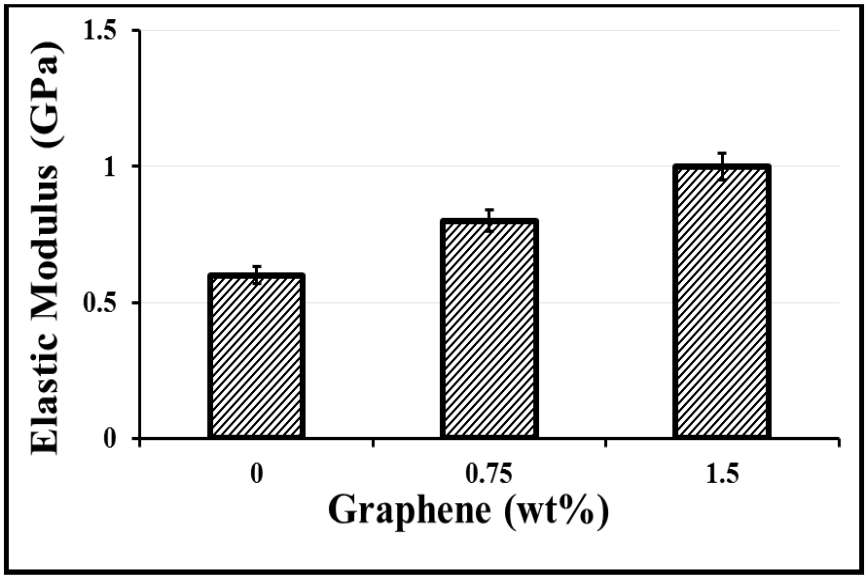

Figure 12. The effect of graphene nanosheets on the modulus of elasticity.

Figure 13 indicates the effect of nanoclay on the modulus of elasticity. As can be seen, the addition of lower weights of nanoclay increases the modulus of elasticity while adding higher weights decreases the modulus of elasticity, which is due to the agglomeration of the nanoparticles.

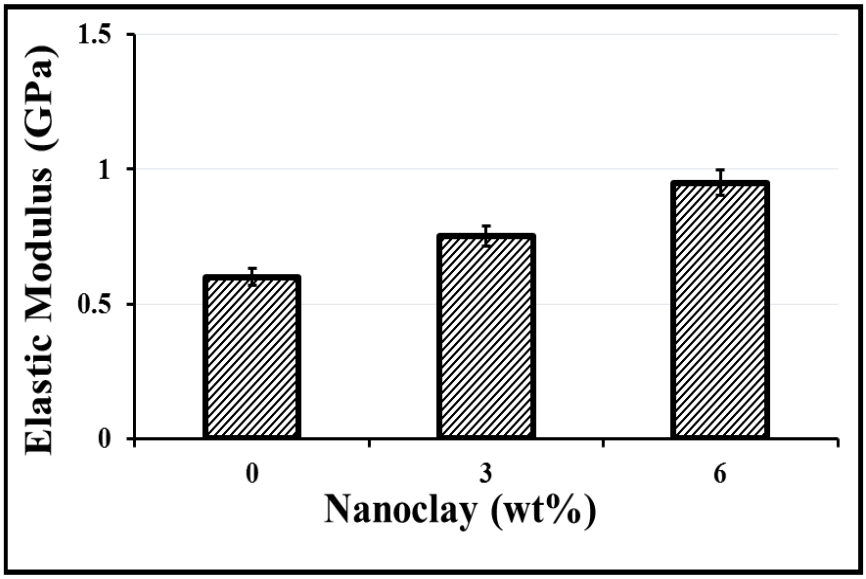

Figure 13. The effect of nanoclay on the modulus of elasticity.

Figure 14 indicates the effect of basalt on the modulus of elasticity. As shown, the incorporation of basalt improved the modulus of elasticity. This is attributable to the higher modulus of basalt than the matrix as well as the loading transfer from the soft polymer matrix to the stiffer fibers.

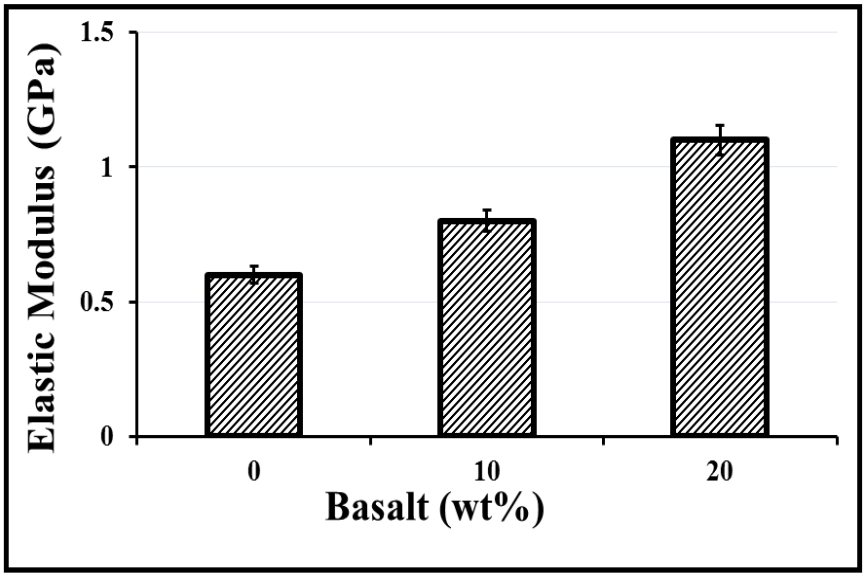

Figure 14. The effect of basalt on the modulus of elasticity.

To determine the significant factors affecting the modulus of elasticity of PP/graphene/nanoclay/basalt hybrid nanocomposites, an ANOVA was run, the results of which were shown in Table 6. As the table shows, all of the three process parameters' linear (graphene, nanoclay, and basalt), square [(graphene × graphene) (nanoclay × nanoclay) (basalt × basalt)], and interaction (nanoclay × basalt) coefficients had an effect on modulus of elasticity based on *p*-value. The high values of R^2 (99.79%), R^2_{Adj} (99.43%), and R^2_{Pred} (97.33%) suggest the strong predictability of the model.

Table 6. ANOVA results for modulus of elasticity.

Source	DF	Adj SS	Adj MS	F	*p*
Model	9	11.24	1.25	270.13	<0.0001
Graphene (A)	1	3.38	3.38	730.81	<0.0001
Nanoclay (B)	1	1.49	1.49	321.69	<0.0001
Basalt (C)	1	5.87	5.87	1268.18	<0.0001
Graphene × Nanoclay (AB)	1	0.0000	0.0000	0.0000	1.0000
Graphene × Basalt (AC)	1	0.0000	0.0000	0.0000	1.0000
Nanoclay × Basalt (BC)	1	0.1056	0.1056	22.84	0.0050
Graphene × Graphene (A^2)	1	0.3186	0.3186	68.89	0.0004
Nanoclay× Nanoclay (B^2)	1	0.0901	0.0901	19.49	0.0069
Basalt × Basalt (C^2)	1	0.0417	0.0417	9.01	0.0300
R^2 = 99.79%		R^2_{Adj} = 99.43%		R^2_{Pred} = 97.33%	

The quadratic equation was shown as an Equation (3) in terms of encoded factors after excluding the small variables.

$$E = 0.2437 + 1.6500A + 0.3021B + 0.12312C - 0.5222A^2 - 0.01736B^2 - 0.001062C^2 - 0.005417BC \quad (3)$$

Figure 15 shows the surface plots and counter plots for modulus of elasticity. Figure 15a indicates the impact of graphene and nanoclay on the modulus of elasticity of the nanocomposite. Figure 15b shows the effect of graphene and basalt, and Figure 15c indicates the impact of nanoclay and basalt on the modulus of elasticity of the nanocomposite.

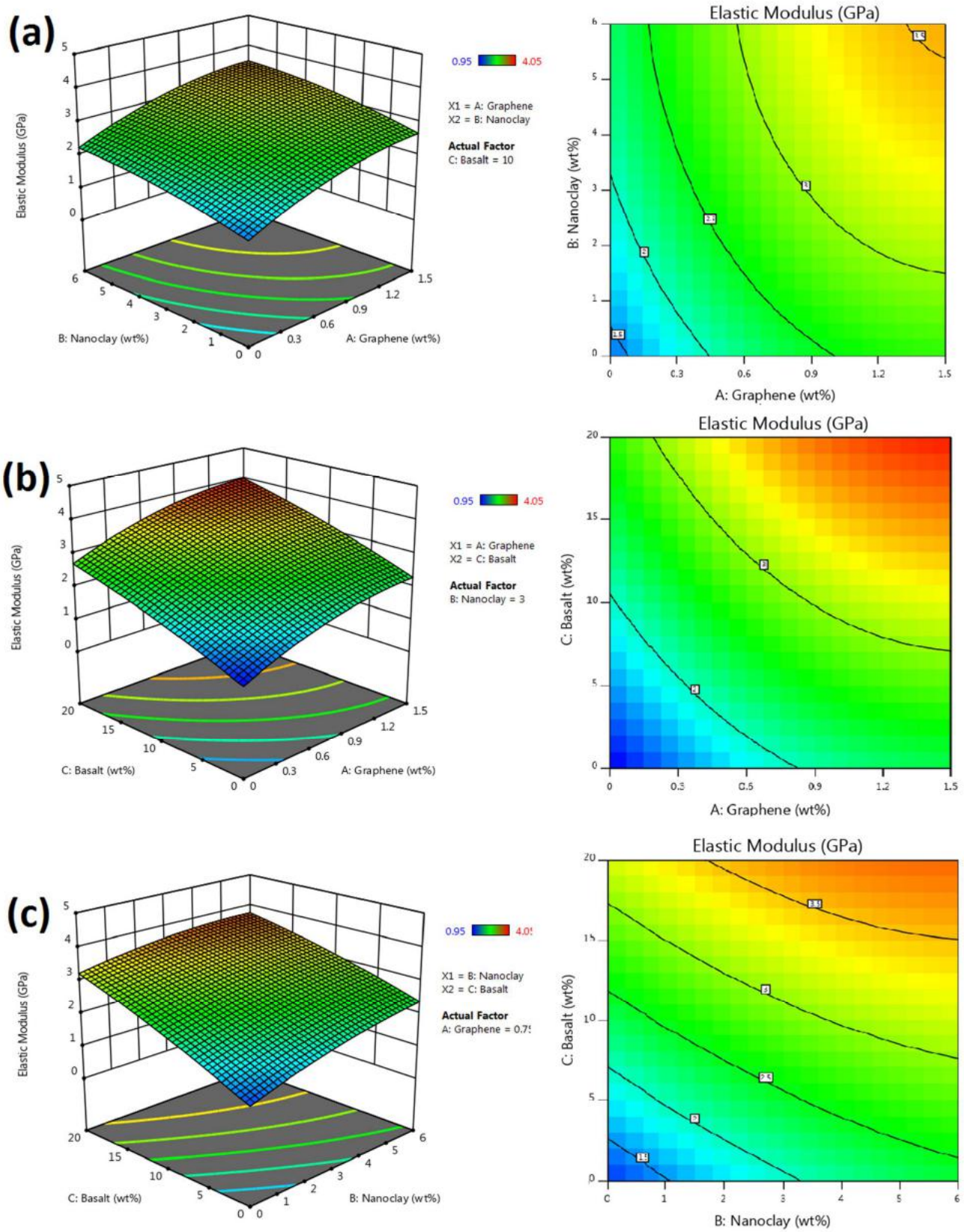

Figure 15. Effect of graphene, nanoclay, and basalt on modulus of elasticity (**a**) Basalt = 10 wt%, (**b**) Nanoclay = 3 wt%, and (**c**) Graphene = 1 wt%.

In Figure 15a, by keeping basalt weight constant at 10 wt%, adding graphene nanoparticles to the compounds increases the modulus of elasticity. This may be attributed to a good

distribution of graphene and their vital role in creating good fiber-matrix adhesion [16]. The inclusion of a lower weight of nanoclay increases the modulus of elasticity while adding it at higher weights decreases the modulus of elasticity, which is due to the agglomeration of the nanoparticles.

In Figure 15b, by keeping nanoclay weight at 3 wt%, increasing basalt increased the modulus of elasticity. This might be attributable to the higher modulus of basalt from the matrix and the effect of loading transfer from the soft polymer matrix to the stiffer fibers. Adding graphene nanoparticles to the compounds increases the modulus of elasticity. This may be attributed to a good distribution of graphene and their effectiveness in creating adhesion between fibers and the matrix [16]. In Figure 15c, by keeping graphene weight at 0.75 wt%, increasing basalt weight improves modulus of elasticity, and adding nanoclay at 3 wt% initially increases the tensile strength and then decreases it.

4.4. Effect of Graphene, Nanoclay, and Basalt on the Impact Strength

Figure 16 shows the effect of graphene on the impact strength. As is evident, the inclusion of graphene at 0.75 wt% enhanced the impact strength owing to the prevention of crack growth in different ways, such as cavitation, bridging, and deflection. However, in samples with 1.5 wt% of graphene, the impact strength decreased.

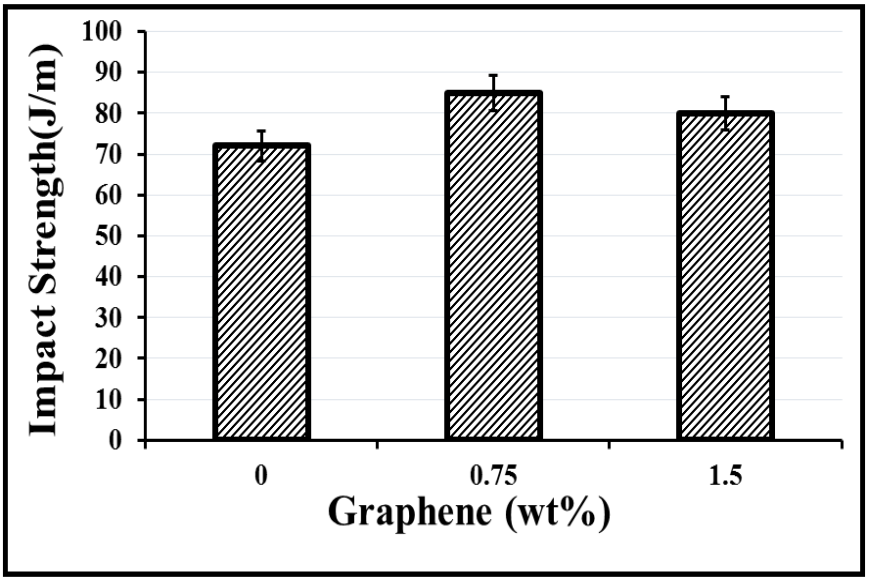

Figure 16. The effect of graphene nanosheets on the impact strength.

Figure 17 shows the effect of nanoclay on the impact strength. As shown, the addition of nanoclay decreased the impact strength and caused nanocomposites to become brittle.

Figure 18 displays the effect of basalt on the impact strength. The improvement in the impact strength by adding basalt fibers is attributable to the strong fiber–matrix adhesion, which restricts fiber pull-out when subjected to impact loading. Also, the applied force is transferred from the matrix to the fibers and causes the fibers to break. The high strength of basalt fibers against fracture, compared to that of pure matrix, enhances the impact strength of nanocomposites [45].

To determine the significant factors affecting the impact strength of PP/graphene/nanoclay/basalt hybrid nanocomposites, an ANOVA was run, the results of which were shown in Table 7. As the table shows, all of the three process parameters' linear (graphene, nanoclay, and basalt), square [(graphene × graphene) (nanoclay × nanoclay) (basalt × basalt)], and interaction (graphene × basalt) coefficients had an effect on modulus of elasticity based on *p*-value. The high values of R^2 (99.54%), R^2_{Adj} (98.71%), and R^2_{Pred} (95.99%) suggest the strong predictability of the model.

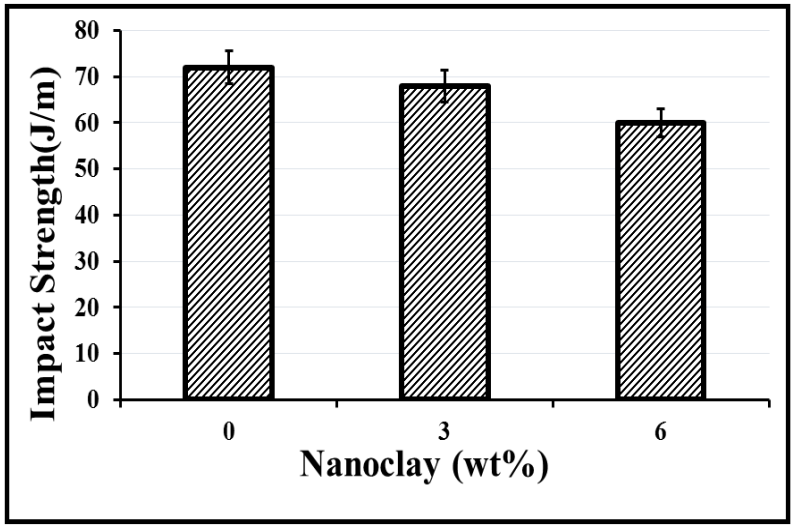

Figure 17. The effect of nanoclay on the impact strength.

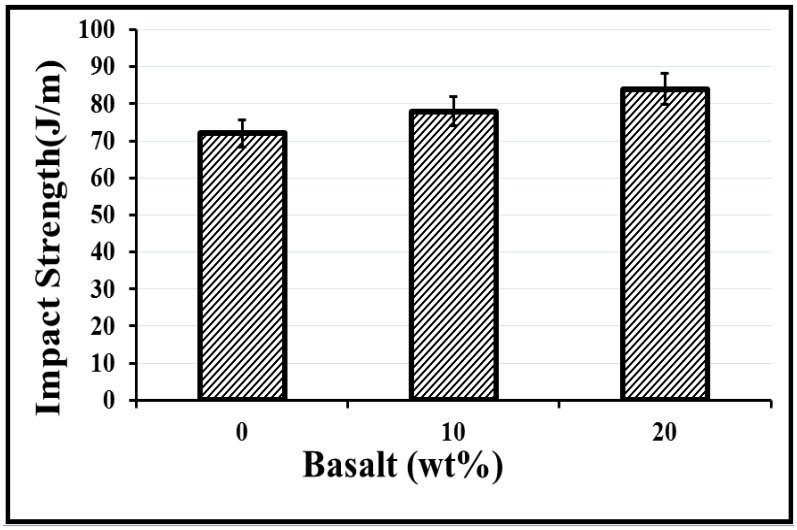

Figure 18. The effect of Basalt on the impact strength.

Table 7. ANOVA results for impact strength.

Source	DF	Adj SS	Adj MS	F	*p*
Model	9	807.18	89.69	119.58	<0.0001
Graphene (A)	1	162.00	162.00	216.00	<0.0001
Nanoclay (B)	1	66.13	66.13	88.17	0.0002
Basalt (C)	1	210.13	210.13	280.17	<0.0001
Graphene × Nanoclay (AB)	1	0.2500	0.2500	0.3333	0.5887
Graphene × Basalt (AC)	1	6.25	6.25	8.33	0.0343
Nanoclay × Basalt (BC)	1	4.00	4.00	5.33	0.0690
Graphene× Graphene (A^2)	1	351.00	351.00	468.00	<0.0001
Nanoclay × Nanoclay (B^2)	1	14.77	14.77	19.69	0.0068
Basalt × Basalt (C^2)	1	8.31	8.31	11.08	0.0208
R^2 = 99.54%		R^2_{Adj} = 98.71%		R^2_{Pred} = 95.99%	

The quadratic equation was shown as an Equation (4) in terms of encoded factors after excluding the small variables.

$$S_I = 68.750 + 33.67A + 0.708B + 1.037C - 17.333A^2 - 0.2222B^2 - 0.01500C^2 - 0.1667AC \quad (4)$$

Figure 19 indicates the surface plots and counter plots for impact strength. Figure 19a displays the effect of graphene and nanoclay on the impact strength of the nanocomposite. Figure 19b shows the impact of graphene and basalt, and Figure 19c illustrates the impact of nanoclay and basalt on the impact strength of the nanocomposite.

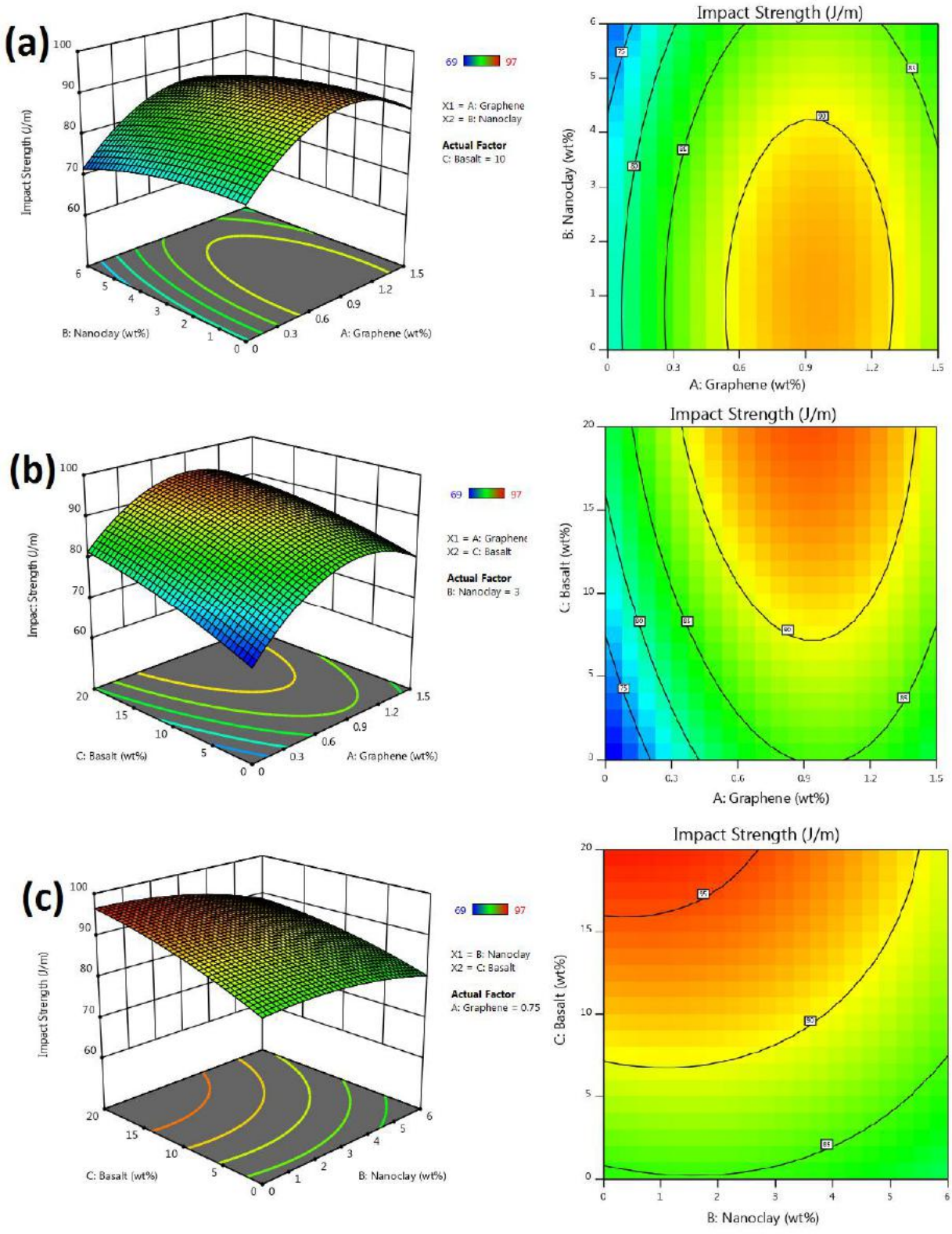

Figure 19. Effect of graphene, nanoclay, and basalt on impact strength (**a**) Basalt = 10 wt%, (**b**) Nanoclay = 3 wt%, and (**c**) Graphene = 1 wt%.

In Figure 19a, by keeping basalt content at 10 wt%, incorporating graphene to 0.75 wt% improved the impact strength, which is ascribed to the creation of different ways to prevent crack growth, such as cavitation, bridging, and deflection by graphene. But, in samples with 1.5 wt% of graphene, the impact strength decreased. Also, the inclusion of nanoclay to the polymer matrix resulted in the formation of a brittle nanocomposite that had low resistance to impact loads. This is due to the brittleness of the compounds after the addition of nanoclay, which causes poor impact strength.

In Figure 19b, by keeping the nanoclay weight at 3 wt%, increasing basalt improved the impact strength, which may be attributed to the strong fiber–matrix adhesion, which prevents fiber pull-out when subjected to impact loading. Also, the applied force is transferred from the matrix to the fibers and causes fiber breakage. The impact strength is increased by adding graphene at 0.75 wt% and reduced by using higher weights of graphene.

In Figure 19c, by maintaining graphene weight at 0.75 wt%, increasing basalt weight increased the impact strength, and adding nanoclay decreased it.

4.5. Optimization of Mechanical Properties

For optimization of the mechanical behavior, the tensile strength, modulus of elasticity, and impact strength must be simultaneously maximized. A viable approach for solving the problem of multiple response optimizations is the use of the desirability function. Drawing on this method, each response equation is first transformed into an individual desirability function (d), varying in the range of $0 \leq d \leq 1$. Based on response characteristics, there are three types of the desirability function:

(1) The higher is better—for an objective function to be maximized;
(2) The lower is better—for an objective to be minimized;
(3) The nominal is better—for an objective function required to achieve a particular target [43].

Here, the tensile strength, modulus of elasticity, and impact strength must be maximized. For this purpose, the associating desirability functions were the-higher-the-better. It can be written in a general form as presented in Equation (5):

$$d = \begin{cases} 0 & y < L \\ \left(\frac{y-L}{T-L}\right)^r & L \leq y \leq T \\ 1 & y > T \end{cases} \quad (5)$$

where y is the response, T is the objective or target of the response, L shows the lower limit of the response and the super index r is the weight factor [49]. When the weight factor is 1, the desirability function will be linear. Selecting $r > 1$ means that it is more important to be close to the target value and choosing $0 \leq r \leq 1$ reduces its importance. Here, as two responses were studied, r = 0.5 was selected.

Depending on the desirability of each response, the component or overall desirability value was then calculated. This component desirability function ($0 \leq D \leq 1$) is optimized (maximized) to locate the optimal factor settings (factor combination). Overall desirability function is given by Equation (6).

$$D = (d_1 d_2 \ldots d_n)^{\frac{1}{n}} \quad (6)$$

where n defines the response number and the desirability function used in this work involved three responses (tensile strength, modulus of elasticity, and impact strength) in a single composite desirability function, which can be written by Equation (7):

$$D = (d_1(tensile\ strength(x)) \times d_2(elastic\ modulus(x) \times d_3(impact\ strength(x))^{\frac{1}{3}} \quad (7)$$

where D denotes the composite desirability function; d_1, d_2 and d_3 are individual desirability functions corresponding to the responses; x is the vector of the designed variables

(coded values); tensile strength(x), modulus of elasticity (x), and impact strength(x) are the predictor of the impact strength and modulus of elasticity given by the regression Equations (2)–(4), respectively.

The results obtained from the desirability function analysis are provided in Figure 20. In this figure, for a simultaneous maximization of the mechanical properties under the best condition of composite desirability (D = 0.95), the graphene should be used at 1.02 wt%, nanoclay at 2.42 wt%, and basalt at 20 wt% (these weight percentages of materials have been suggested after data optimization by Design Expert software). Furthermore, the RSM design of the experiments based on the desirability function predicted that the optimal mechanical behavior can be achieved at the tensile strength of 32.47 MPa, modulus of elasticity of 3.79 GPa, and the impact strength of 95.14 J/m.

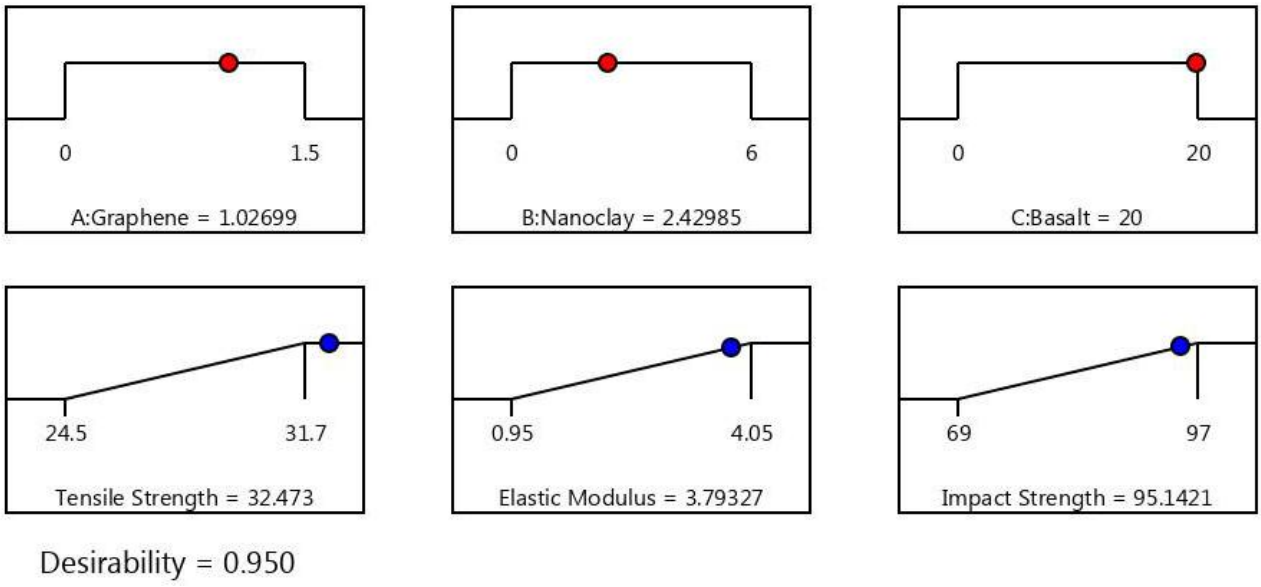

Figure 20. Desirability plot for simultaneous optimization of process parameters.

Moreover, based on the results of the desirability function, the composite desirability (0.95) was fairly close to 1, suggesting that the settings were suitable to yield acceptable results for all the responses.

After optimizing each parameter level with its corresponding response value, a confirmation experiment was conducted in optimal conditions to verify the findings (for the suggested weight percentages, tensile and impact test specimens were made and tensile and impact tests were performed on them). The values obtained by this experiment for the mechanical property were roughly close to the data yielded from desirability optimization, employing RSM (see Table 8).

Table 8. Results of confirmation experiment for optimal conditions.

Mechanical Properties	Prediction	Confirmation Experiment	Error Percent
Tensile strength (MPa)	32.47	32.35	0.34
Modulus of elasticity (GPa)	3.79	3.76	0.62
Impact strength (J/m)	95.14	94.65	0.51

5. Conclusions

In this study, the effect of reinforcement of polypropylene (PP)-based nanocomposites by graphene, nanoclay, and basalt fibers and its impact on tensile and impact properties (tensile strength, modulus of elasticity, and impact strength) was investigated, and the following conclusions were made:

1. The incorporation of 0.75 wt% of graphene improved the tensile strength by 15% owing to better adhesion of fibers to the surface in these samples, but adding 1.5 wt% of these reduced the tensile strength by 3% due to the agglomeration of nanoparticles.
2. The inclusion of 1.5 wt% of graphene increased the modulus of elasticity by 66%. This may be attributed to a good distribution of graphene and their effective role in building a strong fiber–matrix adhesion.
3. The incorporation of 0.75 wt% of graphene enhanced the impact strength by 20%, owing to the prevention of crack growth in different ways, such as cavitation, bridging, and deflection, but the addition of 1.5 wt% of these reduced the impact strength by 7%.
4. Adding 3 wt% of nanoclay improved the tensile strength by 17%, and incorporating 6 wt% reduced the tensile strength by 10% due to the agglomeration of nanoparticles.
5. Adding 6 wt% of nanoclay increased the modulus of elasticity and the impact strength by 59% and reduced the impact strength by 19%, which is due to the agglomeration of the nanoparticles.
6. Adding 20 wt% of basalt improved the tensile strength, modulus of elasticity, and impact strength by 32%, 64%, and 18%, respectively, which may be attributed to the fibers' excellent adhesion to the polymer and no pull-out of the matrix during the mechanical tests, and this is attributable to the higher modulus of basalt than the matrix as well as the loading transfer from the soft polymer matrix to the stiffer fibers.
7. The optimal amount of graphene, nanoclay, and basalt should be at 1.02 wt%, 2.42 wt%, and 20 wt%, respectively, to increase the tensile strength, modulus of elasticity, and impact strength by 48%, 81%, and 39%, respectively.
8. The values obtained by this experiment for the mechanical property were roughly close to the data yielded from desirability optimization.

Author Contributions: Conceptualization, C.T., P.R.S. (Pouyan Roodgar Saffari) and N.R.; methodology, P.R.S. (Pouyan Roodgar Saffari), P.R.S. (Peyman Roudgar Saffari), M.N.N., S.K., S.S.; validation, S.S., C.T. and S.K.; formal analysis, P.R.S. (Pouyan Roodgar Saffari), N.R., P.R.S. (Peyman Roudgar Saffari) and M.N.N.; investigation, P.R.S. (Pouyan Roodgar Saffari), N.R. and C.T.; resources, S.S. and P.R.S. (Peyman Roudgar Saffari); data curation, N.R. and P.R.S. (Pouyan Roodgar Saffari); writing—original draft preparation, C.T. and S.K., P.R.S. (Pouyan Roodgar Saffari), N.R., S.S., M.N.N., P.R.S. (Peyman Roudgar Saffari); writing—review and editing, S.S., C.T., S.K., N.R., M.N.N., P.R.S. (Pouyan Roodgar Saffari) and P.R.S. (Peyman Roudgar Saffari); visualization, C.T., S.K., P.R.S. (Pouyan Roodgar Saffari), N.R., S.S., M.N.N. and P.R.S. (Peyman Roudgar Saffari); project administration, C.T., N.R. and P.R.S. (Pouyan Roodgar Saffari); All authors have read and agreed to the published version of the manuscript.

Funding: This research received no external funding.

Institutional Review Board Statement: Not applicable.

Informed Consent Statement: Not applicable.

Data Availability Statement: The data and materials in this paper are available.

Acknowledgments: This study was supported by Thammasat Postdoctoral Fellowship, Thammasat University Research Division, Thammasat University. Also, This Research was supported by Thammasat University Research Unit in Structural and Foundation Engineering, Thammasat University.

Conflicts of Interest: The authors declare no conflict of interest.

References

1. Moskaleva, A.; Safonov, A.; Hernández-Montes, E. Fiber-Reinforced Polymers in Freeform Structures: A Review. *Adv. Build.* **2021**, *11*, 481. [CrossRef]
2. Zabihi, O.; Ahmadi, M.; Nikafshar, S.; Preyeswary, K.C.; Naebe, M. A technical review on epoxy-clay nanocomposites: Structure, properties, and their applications in fiber reinforced composites. *Compos. Part B Eng.* **2018**, *135*, 1–24. [CrossRef]
3. Selvakumar, V.; Palanikumar, K.; Palanivelu, K. Studies on Mechanical Characterization of Polypropylene/Na^+-MMT Nanocomposites. *J. Miner. Mater. Charact. Eng.* **2010**, *9*, 671–681. [CrossRef]

4. Gabr, M.; Okumura, W.; Ueda, H.; Kuriyama, W.; Uzawa, K.; Kimpara, I. Mechanical and thermal properties of carbon fiber/polypropylene composite filled with nanoclay. *Compos. Part B Eng.* **2015**, *69*, 94–100. [CrossRef]
5. Paul, D.R.; Bucknall, C.B. *Polymer Blends*; Wiley: New York, NY, USA, 2000.
6. Karger-Kocsis, J. Thermoplastic rubbers via dynamic vulcanization. In *Polymer Blends and Alloys*; Shonaike, G.O., Simon, G.P., Eds.; Marcel Dekker: New York, NY, USA, 1999.
7. Seifan, M.; Mendoza, S.; Berenjian, A. A Comparative Study on the Influence of Nano and Micro Particles on the Workability and Mechanical Properties of Mortar Supplemented with Fly Ash. *Adv. Build.* **2021**, *11*, 60. [CrossRef]
8. Zarabimanesh, Y.; Saffari, P.R.; Saffari, P.R.; Refahati, N. Hygro-thermo mechanical vibration of two vertically aligned single-walled boron nitride nanotubes conveying fluid. *J. Vib. Control* **2021**. [CrossRef]
9. Roodgar Saffari, P.; Fakhraie, M.; Roudbari, M.A. Size-Dependent Vibration Problem of Two Vertically-Aligned Single-Walled Boron Nitride Nanotubes Conveying Fluid in Thermal Environment via Nonlocal Strain Gradient Shell Model. *J. Solid Mech.* **2021**, *13*, 164–185. [CrossRef]
10. Saffari, P.R.; Fakhraie, M.; Roudbari, M.A. Free vibration problem of fluid conveying double-walled boron nitride nanotubes via nonlocal strain gradient theory in thermal environment. *J. Mech. Based Des. Struct. Mach.* **2020**, *234*, 1–18. [CrossRef]
11. Roodgar Saffari, P.; Fakhraie, M.; Roudbari, M.A. Free Vibration and Transient Response of Heterogeneous Piezoelectric Sandwich Annular Plate Using Third-Order Shear Deformation Assumption. *J. Solid Mech.* **2020**, *12*, 315–333. [CrossRef]
12. Saffari, P.R.; Fakhraie, M.; Roudbari, M.A. Nonlinear vibration of fluid conveying cantilever nanotube resting on visco Pasternak foundation using non-local strain gradient theory. *Micro Nano Lett.* **2020**, *15*, 181–186. [CrossRef]
13. Nadiv, R.; Shtein, M.; Buzaglo, M.; Peretz-Damari, S.; Kovalchuk, A.; Wang, T.; Tour, J.M.; Regev, O. Graphene nanoribbon—Polymer composites: The critical role of edge functionalization. *Carbon* **2016**, *99*, 444–450. [CrossRef]
14. Shokrieh, M.M.; Ahmadi Joneidi, V. Manufacturing and experimental characterization of Graphene/ Polypropylene nanocomposites. *Modares Mech. Eng.* **2014**, *13*, 55–63.
15. Feng, Z.; Li, Y.; Xin, C.; Tang, D.; Xiong, W.; Zhang, H. Fabrication of Graphene-Reinforced Nanocomposites with Improved Fracture Toughness in Net Shape for Complex 3D Structures via Digital Light Processing. *Carbon Res.* **2019**, *5*, 25. [CrossRef]
16. YetkİN, S.H.; KaradenİZ, B.; Güleşen, M. Investigation of the Mechanical and Thermal Properties of Graphene Oxide Filled Polypropylene Composites. *Araştırma Makalesi* **2017**, *4*, 34–40.
17. Wang, J.; Song, F.; Ding, Y.; Shao, M. The incorporation of graphene to enhance mechanical properties of polypropylene self-reinforced polymer composites. *Mater. Des.* **2020**, *195*, 109073. [CrossRef]
18. Ansari, M.J.; Jabbaripour, B. Manufacture and Comparison of Mechanical Properties of Reinforced Polypropylene nanocomposite with Carbon Fibers and Calcium Carbonate Nanoparticles. *Iran. J. Manuf. Eng.* **2019**, *6*, 1–12.
19. Yuan, B.; Bao, C.; Song, L.; Hong, N.; Liew, K.M.; Hu, Y. Preparation of functionalized graphene oxide/polypropylene nanocomposite with significantly improved thermal stability and studies on the crystallization behavior and mechanical properties. *Chem. Eng. J.* **2014**, *237*, 411–420. [CrossRef]
20. Gharebeiglou, M.; Izadkhah, M.S.; Erfan-Niya, H.; Entezami, A.A. Improving the mechanical and thermal properties of chemically modified graphene oxide/polypropylene nanocomposite. *Modares Mech. Eng.* **2016**, *16*, 196–206.
21. Hadadi Asl, V.; Karimkhani, V. *Introduction to Nanotechnology Applications in Polymers*; Petroleum Industry Research Center: Tehran, Iran, 2010; pp. 165–178.
22. Rahmani, R.; Ghorbanpoor Arani, A.; Shokravi, M. *Introduction to Nanotechnology*; Academic Book Publishing: Tehran, Iran, 2009; pp. 300–304.
23. Bidi, A.; Liaghat, G.; Rahimi, G. Effect of nano clay addition to energy absorption capacity of steel-polyurea bi-layer. *J. Sci. Technol. Compos.* **2016**, *3*, 157–164.
24. Esmizadeh, E.; Sahraeian, R.; Naderi, G.; Esfandeh, M. Mechanical behavior of nanoperlite/ nanoclay hybrid nanocomposites based on polyethylene. *J. Sci. Technol. Compos.* **2019**, *6*, 283–293.
25. Bheel, N.; Tafsirojjaman, T.; Liu, Y.; Awoyera, P.; Kumar, A.; Keerio, M.A. Experimental Study on Engineering Properties of Cement Concrete Reinforced with Nylon and Jute Fibers. *Adv. Build.* **2021**, *11*, 454. [CrossRef]
26. Gravit, M.; Golub, E.; Klementev, B.; Dmitriev, I. Fire Protective Glass Fiber Reinforced Concrete Plates for Steel Structures under Different Types of Fire Exposure. *Adv. Build.* **2021**, *11*, 187. [CrossRef]
27. Mina, A.; Petrou, M.; Trezos, K. Resistance of an Optimized Ultra-High Performance Fiber Reinforced Concrete to Projectile Impact. *Adv. Build.* **2021**, *11*, 63. [CrossRef]
28. Mostafa, M.; Uddin, N. Effect of Banana Fibers on the Compressive and Flexural Strength of Compressed Earth Blocks. *Buildings* **2015**, *5*, 282–296. [CrossRef]
29. Stepien, A.; Kostrzewa, P. The Impact of Basalt Components on the Structure of Bricks Formed as a Result of Hydrothermal Treatment. *Buildings* **2019**, *9*, 192. [CrossRef]
30. Wu, Z.; Wang, X.; Liu, J. *Handbook of Natural Fibres: Chapter 13*, 2nd ed.; Woodhead Publishing: Cambridge, UK, 2020; pp. 433–502.
31. Balaji, K.V.; Shirvanimoghaddam, K.; Rajan, G.S.; Ellis, A.V.; Naebe, M. Surface treatment of Basalt for use in automotive composites. *J. Mater. Today Chem.* **2020**, *17*, 100334. [CrossRef]
32. Lopresto, V.; Leone, C.; De Iorio, I. Mechanical characterisation of basalt fibre reinforced plastic. *Compos. Part B Eng.* **2011**, *42*, 717–723. [CrossRef]

33. Wu, G.; Wang, X.; Wu, Z.; Dong, Z.; Zhang, G. Durability of basalts and composites in corrosive environments. *J. Compos. Mater.* **2015**, *49*, 873–887. [CrossRef]
34. Colombo, C.; Vergani, L.; Burman, M. Static and fatigue characterisation of new basalt fibre reinforced composites. *Compos. Struct.* **2012**, *94*, 1165–1174. [CrossRef]
35. High, C.; Seliem, H.M.; El-Safty, A.; Rizkalla, S.H. Use of basalt fibers for concrete structures. *Constr. Build. Mater.* **2015**, *96*, 37–46. [CrossRef]
36. Shishevan, F.A.; Akbulut, H.; Mohtadi-Bonab, M.A. Low velocity impact behavior of basalt fiber-reinforced polymer composites. *J. Mater. Eng. Perform.* **2017**, *26*, 2890–2900. [CrossRef]
37. Safiuddin, M.; Abdel-Sayed, G.; Hearn, N. Absorption and Strength Properties of Short Carbon Fiber Reinforced Mortar Composite. *Buildings* **2021**, *11*, 300. [CrossRef]
38. Ralegaonkar, R.; Gavali, H.; Aswath, P.; Abolmaali, S. Application of chopped basalt fibers in reinforced mortar: A review. *Constr. Build. Mater.* **2018**, *164*, 589–602. [CrossRef]
39. Eslami-Farsani, R.; Khalili, S.M.R.; Hedayatnasab, Z.; Soleimani, N. Influence of thermal conditions on the tensile properties of basalt fiber reinforced polypropylene—clay nanocomposites. *Mater. Des.* **2014**, *53*, 540–549. [CrossRef]
40. Chen, W.; Hao, H.; Jong, M.; Cui, J.; Shi, Y.; Chen, L.; Pham, T. Quasi-static and dynamic tensile properties of basalt fi bre reinforced polymer. *Compos. Part B Eng.* **2017**, *125*, 123–133. [CrossRef]
41. Menbari, S.; Ashenai Ghasemi, F.; Ghasemi, I. Comparison of mechanical properities of hybrid nanocomposites of Polypropylene/Talc/Graphene with Polypropylene/Graphene. *Modares Mech. Eng.* **2015**, *15*, 329–335.
42. Mirzaei, J.; Fereidoon, A.; Ghasemi-Ghalebahman, A. Experimental analysis of graphene nanoparticles and glass fiber effect on mechanical and thermal properties of polypropylene/EPDM based nanocomposites. *J. Sci. Technol. Compos.* **2018**, *5*, 169–176.
43. Montgomery, D.C. *Design and Analysis of Experiments*; J. Wiley Sons: New York, NY, USA, 2005.
44. Ghasemi, F.A.; Niyaraki, M.N.; Ghasemi, I.; Daneshpayeh, S. Predicting the tensile strength and elongation at break of PP/graphene/glass fiber/EPDM nanocomposites using response surface methodology. *Mech. Adv. Mater. Struct.* **2021**, *28*, 981–989. [CrossRef]
45. Hassan, M.Z.; Sapuan, S.; Roslan, S.A.; Sarip, S. Optimization of tensile behavior of banana pseudo-stem (Musa acuminate) fiber reinforced epoxy composites using response surface methodology. *J. Mater. Res. Technol.* **2019**, *8*, 3517–3528. [CrossRef]
46. Choudhary, V.; Varma, H.; Varma, I. Polyolefin blends: Effect of EPDM rubber on crystallization, morphology and mechanical properties of polypropylene/EPDM blends. *Polymer* **1991**, *32*, 2534–2540. [CrossRef]
47. Sukur, E.F.; Onal, G. Graphene nanoplatelet modified basalt/epoxy multi-scale composites with improved tribological performance. *J. Wear* **2020**, *460–461*, 203481. [CrossRef]
48. Idumah, C.I.; Hassan, A. Characterization and preparation of conductive exfoliated graphene nanoplatelets kenaf fibre hybrid polypropylene composites. *J. Synth. Met.* **2016**, *212*, 91–104. [CrossRef]
49. George, E.; Hunter, J.S.; Hunter, W.G. *Statistics for Experimenters: Design, Innovation and Discovery*, 4th ed.; John Wiley and Sons: New York, NY, USA, 2005.